# Prompt gamma measurements for locating the dose falloff region in the proton therapy

Cite as: Appl. Phys. Lett. **89**, 183517 (2006); https://doi.org/10.1063/1.2378561
Submitted: 04 July 2006 • Accepted: 20 September 2006 • Published Online: 02 November 2006

**Chul-Hee Min, Chan Hyeong Kim, Min-Young Youn, et al.**

# Prompt gamma measurements for locating the dose falloff region in the proton therapy

Chul-Hee Min and Chan Hyeong Kim
*Department of Nuclear Engineering, Hanyang University, 17 Haengdang, Sungdong, Seoul 133-791, Korea*

Min-Young Youn
*National Center for Inter-University Research Facility, Seoul National University, Sillim, Gwanak, Seoul 151-742, Korea*

Jong-Won Kim[a)]
*Department of Biomedical Engineering, National Cancer Center, 809 Madu, Koyang, Kyonggi 411-764, Korea*

(Received 4 July 2006; accepted 20 September 2006; published online 2 November 2006)

The location of the distal falloff in the proton therapy is an important but often uncertain parameter as different tissue elements are traversed by the beam. A multilayered collimator system has been constructed as a practical means to locate the dose ends by measuring prompt gammas. The collimator is designed to moderate and capture fast neutrons and to prevent unwanted gammas from reaching the scintillation detector. The system has been studied using Monte Carlo technique and has been tested in the beam energy range of 100–200 MeV. Measurements clearly indicated correlations between the gamma distributions and the distal falloff regions. © *2006 American Institute of Physics*. [DOI: 10.1063/1.2378561]

Proton beam therapy is a high-quality radiation therapy modality in terms of precise dose deposit to the tumor volume prescribed in a cancer patient.[1–3] Hadron beams in general have an advantage in the dose distribution over conventional radiation modalities such as 6–20 MeV photons due to the presence of a Bragg peak. The photons inherently deposit higher integrated doses in the normal tissue of a patients body compared to the protons.[4] The higher dose at the Bragg peak is the result of the increase in the stopping power or energy deposit per unit length inversely proportional to the square of the ion velocity as expressed by the Bethe-Bloch formula.[5] These characteristics of the proton beam therapy result in reducing unnecessary dose to the normal tissues. However, this advantage takes some risks in that the critical tissue located near the end of the proton range can be subject to receiving under- or overdoses if the range is not accurately known. In the planning of radiation treatments the most usual method of defining the ranges is based on the information of electron density distributions attained from the CT images. Hence, it is difficult to fully consider complicated atomic compositions of different tissue elements, which makes the proton range uncertain even to the extent of 1–2 cm.[6] To fully utilize the beneficial physical properties of a proton beam, it is often required to irradiate the tumor region in a precision better than 1–2 mm.

Unlike the photons of conventional radiation therapy, the therapeutic proton or heavier ion beams stop inside the treatment volume, and thus it is not feasible to directly detect the end of the dose deposit. To monitor the range it is needed to detect gammas emitted from nuclear reactions, and there are two kinds of gammas that can be used: (1) coincident gammas from the production of positron emission isotopes and (2) prompt gammas from excitations of the target nuclei by the proton bombardment. The former method provides the same resolution and image quality of positron emission tomography (PET), and has been tested for the carbon beam therapy.[7,8] However, the proton beam has a different mechanism in producing the PET isotopes; i.e., activity of positron emitters is induced in the target nuclei, while fragments of the projectile nuclei are the main sources of activities in the heavy ion therapy. Consequently for the proton therapy, the dose distribution determined by the energy deposit mismatches with the distribution of the isotopes by nuclear reaction. Also, it has been observed that the time lag between treatment and PET scanning can affect determination of the range presumably due to the isotopes of different half-lives.[9] However, a direct comparison between the convolution image by more sophisticated Monte Carlo simulation and the PET signal may reveal the range more accurately.[10] The prompt gammas, on the other hand, are generated by various interaction mechanisms of a proton beam with a target being characterized by the decay time much less than 1 s. In the case of water phantom the prompt gammas come from the interaction with oxygen.

The use of prompt gammas has been suggested to correlate with the distal falloff,[11,12] which was based on Monte Carlo simulation results using GEANT (Ref. 13) or MCNPX,[14] but no attempt of experimental study has been made before. The principle is simple that the range can be determined by counting the gammas emitted from the 90° of the beam direction as depicted in Fig. 1. We chose the design of the collimator to suppress fast neutrons and to select gammas passing only the collimation hole. The high-energy spallation neutrons are the major background deterring the signal gammas. These are highly forward oriented, but still strong enough to compete with the signal collected at 90° if not adequately shielded. The prompt gamma scanner (PGS) consists of three layers of shielding against neutrons generated from the phantom. The paraffin layer moderates the high-energy neutrons, the $B_4C$ powder capturing the neutrons by the $B(n,\gamma)$ reaction, and finally the lead layer blocking the

a)Electronic mail: jwkim@ncc.re.kr

 

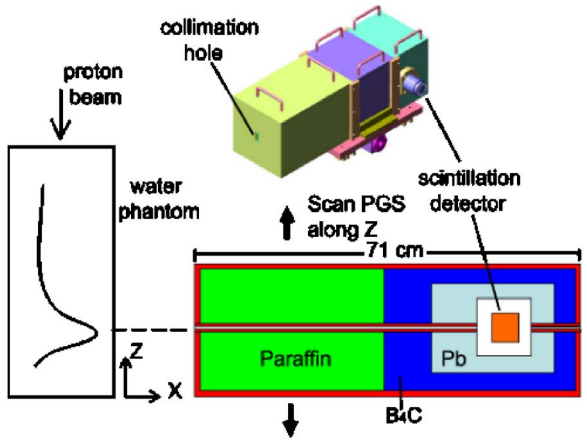


FIG. 1. (Color online) Isomeric and sectional views of the collimator whose dimensions were chosen after a series of Monte Carlo simulations. The collimation hole is located near the Bragg peak to detect the dose falloff region.

unwanted gammas. The gamma detector is a CsI(Tl) scintillator (Scionix, Holland) whose dimensions were determined as $15\times30\times40$ mm$^3$ to match with the collimation hole ($4\times30$ mm$^2$) and to have a longer interaction length along the collimation direction. The signal from the photomultiplier tube is preamplified and analyzed with a multichannel analyzer (MCA) (ULS 1202) placed near the detector. The data are transferred to the computer outside of the experimental area through the parallel port.

To find out the relationship with the actual dose distribution the gamma measurements were compared to the depth-dose distributions measured using a parallel-plate ionization chamber (Marcus chamber, PTW type 23343) at three different proton energies in water phantom, as shown in Fig. 2. We added a 4-cm-thick layer of paraffin plates surrounding the PGS for those measurements, and its effects were revealed later. The beam energies were approximately 100, 150, and 150 MeV, and the exact energies deviated by the energy degradation with the passages of the beam profile monitors, the vacuum window made of Plexiglas, and so on. It is clearly shown that the peaks of prompt gamma distributions are well correlated with the Bragg peaks of the dose distributions, e.g., within 1–2 mm at 100 MeV. The sharpness of the gamma distributions in the distal falloff diminished at higher energies because higher energy neutrons blurred the signal, which was also expected from the simulation study using MCNPX. The gamma counting on Fig. 2 was performed by summing the gammas of over 4 MeV, and each measurement was done for 10 s at the beam current of roughly 2 nA. The reason for choosing 4 MeV is explained later. The MCA was energy calibrated using the 661.6 and 1173+1332 keV gamma peaks of $^{137}$Cs and $^{60}$Co sources, respectively. Measurements were performed at the experimental area of the proton therapy facility in the National Cancer Center of Korea.[15]

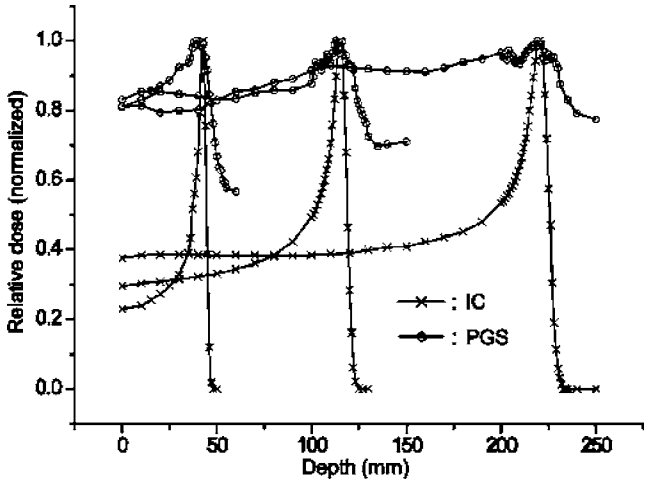


FIG. 2. Comparisons of the depth-dose distributions measured by the ionization chamber with the PGS measurements at three different proton energies of 100, 150, and 200 MeV.

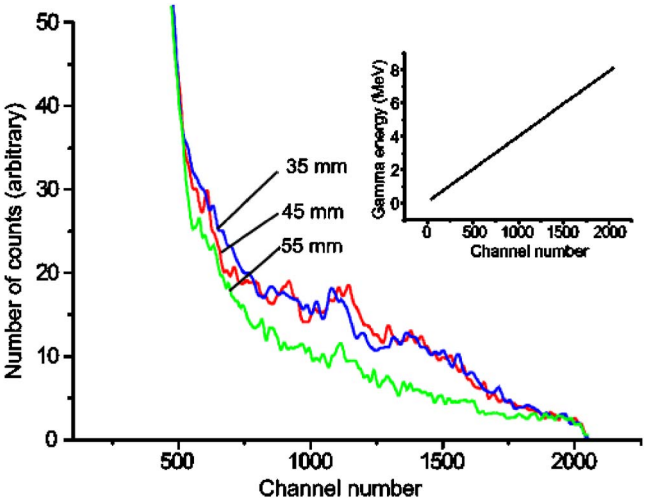


FIG. 3. (Color online) Gamma-energy spectrum measured at three different locations adjacent to the Bragg peak at the proton energy of 100 MeV. The 45 mm location is near the peak. The inset is the energy calibration curve for the MCA.

Figure 3 shows three gamma-energy spectra attained at three locations before, near, and after the Bragg peak along the water phantom in the case of 100 MeV. The inset indicates that the channel number of 500 approximately corresponds to the energy of 2 MeV and 1000 to 4 MeV. Each spectrum was measured for the same time period of 180 s. There is a considerable decrease in the gamma counting in the downstream of the peak.

We chose the minimum gamma energy of 4 MeV in counting based on the results shown in Fig. 4 at the beam energy of 150 MeV, which is a plot of gamma-count distribution with a variation of minimum energy. The deepest fall-

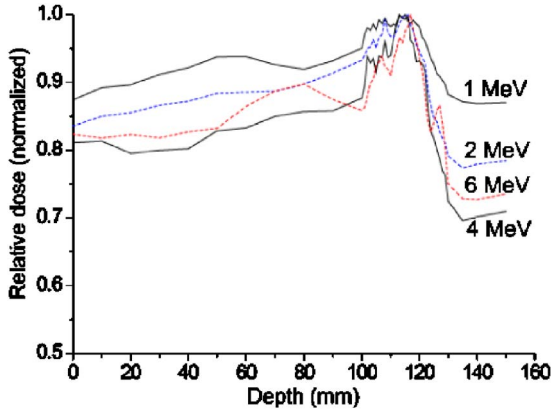


FIG. 4. (Color online) Gamma-count distributions vs depth with different minimum gamma energies set as indicated.

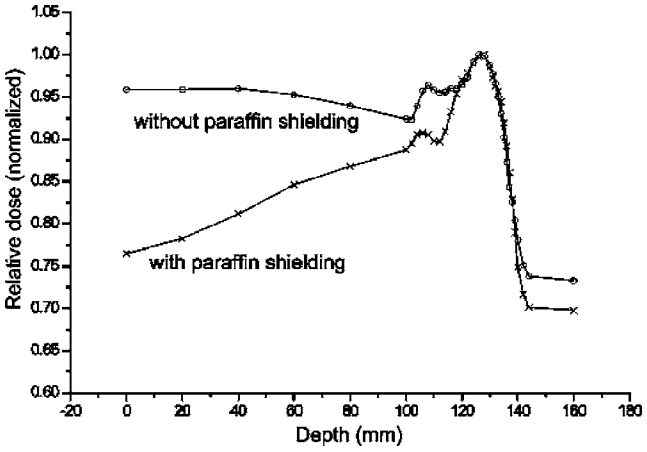


FIG. 5. Gamma-count distributions vs depth with and without paraffin shielding plates surrounding the outside of the PGS.

off was attained for the 4 MeV case, and the same trend was observed at the beam energies of 100 and 200 MeV. The gamma energies for the major decay channels start above 2 MeV.[16] The higher minimum energy may be acceptable, but has a shortcoming in requiring a longer collection time to meet the statistics, while the lower cutoff energy is more susceptible to background noise.

We measured gammas after detaching 4-cm-thick paraffin plates from the outside of the PGS. A comparison was then made between with and without paraffin plates, as shown in Fig. 5. The paraffin layer reduces scintillation counts quite significantly in the upstream of the dose falloff region. This effect is thought to occur partly with better shielding of scattered neutrons from the walls of the experimental area by the additional paraffin layer, and will certainly appear in the real treatment rooms as their walls are closely placed around a patient. However, it has no influence on locating the dose falloff region.

The current results reveal that the prompt gammas generated by nuclear reactions can be used to verify the proton range in the proton radiation therapy. Especially for passive therapeutic beams formed using scatterers and compensator,[17] the PGS could be used to find out the distal falloff by scanning the device near the expected dose-end location. Verification of the longest range by the prompt gamma measurements is expected to be clinically useful for ensuring the tuning of proton energy and the ranges computed from the treatment planning. The three-dimensional contour of the distal dose ends formed by the compensator is rigidly defined so as not to be confirmed *in situ*. However, the general applicability for arbitrary compensators needs to be looked at in future studies because the method envisioned will more likely work for small fields such as in radiotherapy, where the distal contour is smooth. This gamma measurement could also be used to verify the accuracy of the fractionated beam delivery in each treatment session. The spread-out Bragg peaks, which are the actual dose profiles for the therapy, should not affect the gamma-count falloff near the uppermost end of the dose because each gamma spectrum is measured for more than a second while individual pristine Bragg peak is repeatedly formed at over 10 Hz. However, this technique requires improvement for a moving (scanning) beam, which is a more advanced method in the delivery of therapeutic proton beams.[2] In principle it is feasible to make multiple collimation slots such as in the gamma camera and use position sensitive gamma detectors with a larger aperture at the cost of a more complicated system, but it needs further simulation study and refinements. With the experimental confirmation of the prompt gamma distribution correlated with the distal falloff, we plan to devise a more practical configuration for the verification of the proton range, which should help in assuring the quality of proton beam therapy.

This research work is performed under the user program of proton engineering frontier project and basic atomic energy research institute supported by the Ministry of Science and Technology of Korea.

[1] R. Wilson, Radiology **47**, 487 (1946).
[2] A. Boyer, M. Goitein, A. Lomax, and E. Pedroni, Phys. Today **55**(9), 34 (2002).
[3] W. Weyrather and J. Debus, Clin. Oncol. **15**, S23 (2003).
[4] H. Suit and D. Phil, Int. J. Radiat. Oncol., Biol., Phys. **53**, 798 (2002).
[5] H. Bethe, Phys. Rev. **89**, 1256 (1953).
[6] U. Schneider and E. Pedroni, Med. Phys. **22**, 353 (1995).
[7] K. Parodi and W. Enghart, Phys. Med. Biol. **45**, N151 (2000).
[8] A. Paans and J. Schippers, IEEE Trans. Nucl. Sci. **40**, 1041 (1993).
[9] T. Nishio, T. Sato, H. Kitamura, K. Murakami, and T. Ogino, Med. Phys. **32**, 1070 (2005).
[10] K. Parodi and T. Bortfeld, Phys. Med. Biol. **51**, 1991 (2006).
[11] F. Stichelbaut, Y. Jongen, Meeting of the 39th Particle Therapy Cooperative Group, San Francisco, October 2003 (unpublished).
[12] K. Seo, C. Kim, and J. Kim, J. Korean Phys. Soc. **48**, 855 (2006).
[13] GEANT, Detector description and simulation tool, CERN Program Library Long Write-Up W5013, CERN, Geneva.
[14] MCNPX Version 2.4.0 User's Manual; Los Alamos National Laboratory Report No. LA-CP-02-408, 2002 (unpublished).
[15] J. Kim, J. Korean Phys. Soc. **43**, S50 (2003).
[16] B. Kozlovsky, R. Murphy, and R. Ramaty, Astrophys. J., Suppl. Ser. **141**, 523 (2002).
[17] W. Chu, B. Ludewigt, and T. Renner, Rev. Sci. Instrum. **64**, 2055 (1993).